Electronic Supporting Information (ESI) for:

Bottom-up Excited State Dynamics of Two Cinnamate-Based Sunscreen Filter Molecules

Yoann Peperstraete,[a,b] Michael Staniforth,[a] Lewis A. Baker,[a] Natércia D. N. Rodrigues,[a] Neil C. Cole-Filipiak,[a] Wen-Dong Quan[a] and Vasilios G. Stavros[a]

[a]University of Warwick, Gibbet Hill Road, Coventry CV4 7AL, U.K.
[b]ENS de Cachan, 61 Avenue du Président Wilson, 94230 Cachan, France.

I. Isomers of MMC

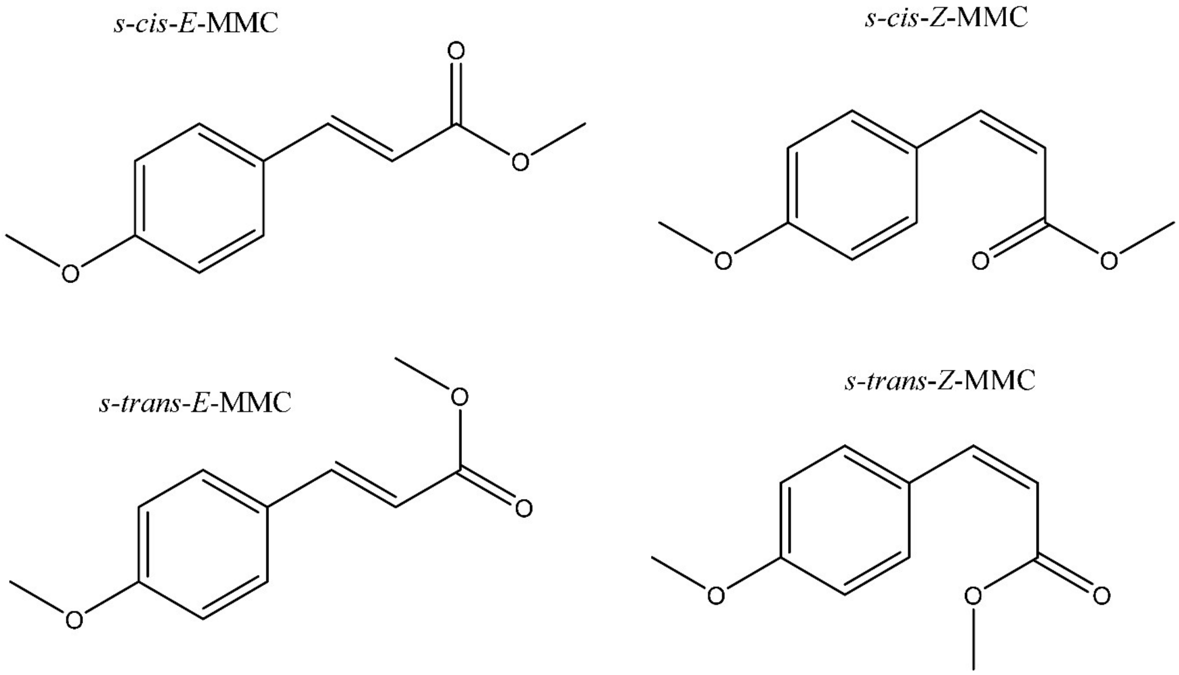

Figure 1: Molecular structures of the different isomers of MMC considered in the present study.[1]

---

[1] E. M. M. Tan, M. Hilbers and W. J. Buma, *J. Phys. Chem. Lett.*, 2014, **5**, 2464.

II. Determination of gas-phase instrument response

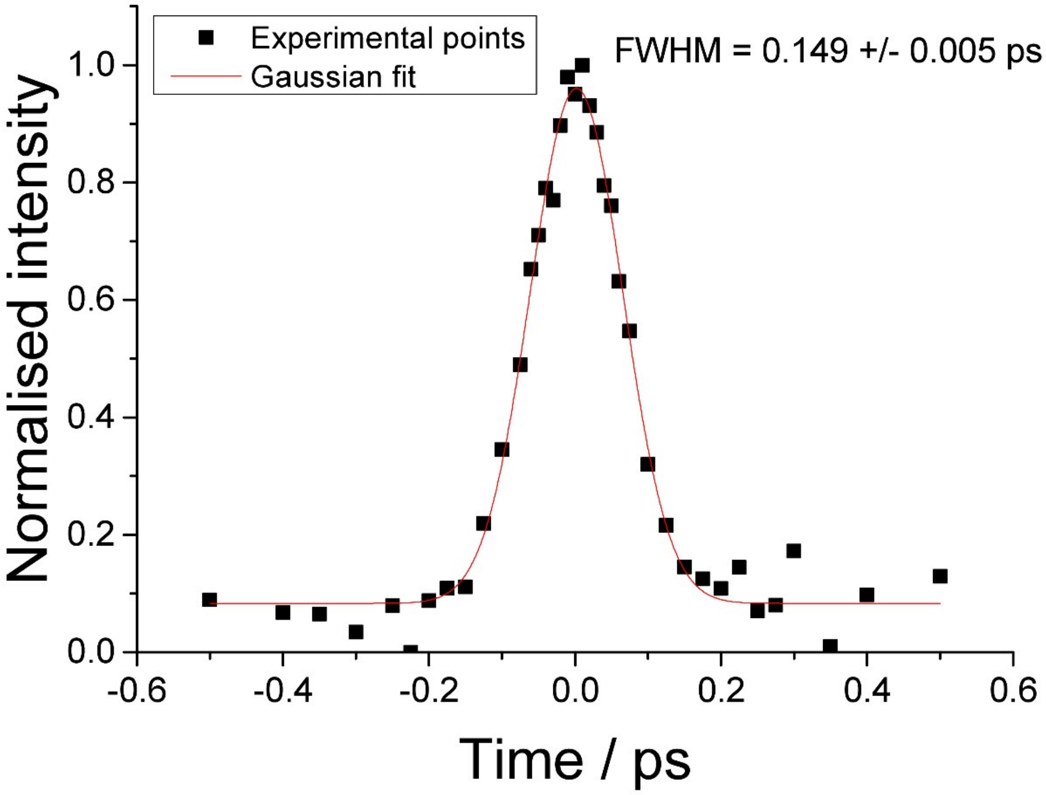

Figure 2: Representative experimental instrument response and Gaussian fit obtained when using the 290 nm pump and the 200 nm probe in Xe; estimated time resolution ~150 fs.

To estimate our temporal resolution, we ran a time-resolved ion yield (TR-IY) scan of Xe^+ with the corresponding photoexcitation/probe wavelengths used in the present measurements. As Xe has no dynamics at these photoexcitation wavelengths (at least within our temporal resolution), this enabled us to extract the instrumental response, a representative of which is shown on Figure 2.

III. Kinetic analysis of gas-phase TR-IY transients and solution-phase TAS

To fit the dynamics observed in the gas-phase, we used a time dependent function, $f(t)$. This function is the sum of a constant baseline offset, y_0, and the convolution products of a Gaussian (centred at time zero, t_0, and with a full width at half maximum, FWHM, of G, see section II) with exponential decays having amplitudes *A* and time constants τ:

$$f(t) = y_0 + \sum_{i=1}^{n}\left[A_i \times e^{\left(\frac{G}{2\times\tau_i\times1.665109}\right)^2 - \frac{t-t_0}{\tau_i}} \times \left(1 - erf\left(\frac{G}{2\times\tau_i\times1.665109} - \frac{1.665109\times(t-t_0)}{G}\right)\right)\right]$$
$$+ \sum_{i=1}^{n'}\left[A_{rev,i} \times e^{\left(\frac{G}{2\times\tau_{rev,i}\times1.665109}\right)^2 + \frac{t-t_0}{\tau_{rev,i}}} \times \left(1 - erf\left(\frac{G}{2\times\tau_{rev,i}\times1.665109} + \frac{1.665109\times(t-t_0)}{G}\right)\right)\right]$$

where $4 * ln(2) \simeq 1.665109$ and $1 - erf(z)$ is the complementary error function. The first and second sums correspond, respectively, to the forward dynamics (pump-probe dynamics) and the reverse dynamics (probe-pump dynamics): n and n' are the numbers of exponential decays used in the fit relative to the forward and reverse dynamics respectively. Moreover, the position of t_0 is a parameter which is allowed to float in the fits and is not determined experimentally. The reason is that, for both *E*-MMC and *E*-EHMC, the low-power conditions used to generate the TR-IY transients do not provide enough Xe^+ signal, when using Xe, to do a cross-correlation (same as section II) and, then, extract the position of t_0 experimentally.

In the solution-phase, the global fitting of the transient absorption spectra, TAS, is also carried out using the sum of the convolution products of a Gaussian, $G(t)$, (centred at time zero, t_0, see section IV) with exponential decays having amplitudes *A* and time constants τ. The fitting function is then:

$$f(t) = \sum_{i=1}^{n}\left[G(t) * \left(A_i(\lambda) \times e^{-\frac{t-t_0}{\tau_i}}\right)\right]$$

where n is the number of exponential decays used in the fit relative to the forward dynamics (no reverse dynamics are used in the solution-phase fits). Again, the position of t_0 is a parameter allowed to float in the fits and is not determined experimentally. The plot of the amplitudes (A_i) against the probe wavelength (λ) corresponds to the decay associated spectra, DAS.

IV. Determination of the solution-phase instrument response

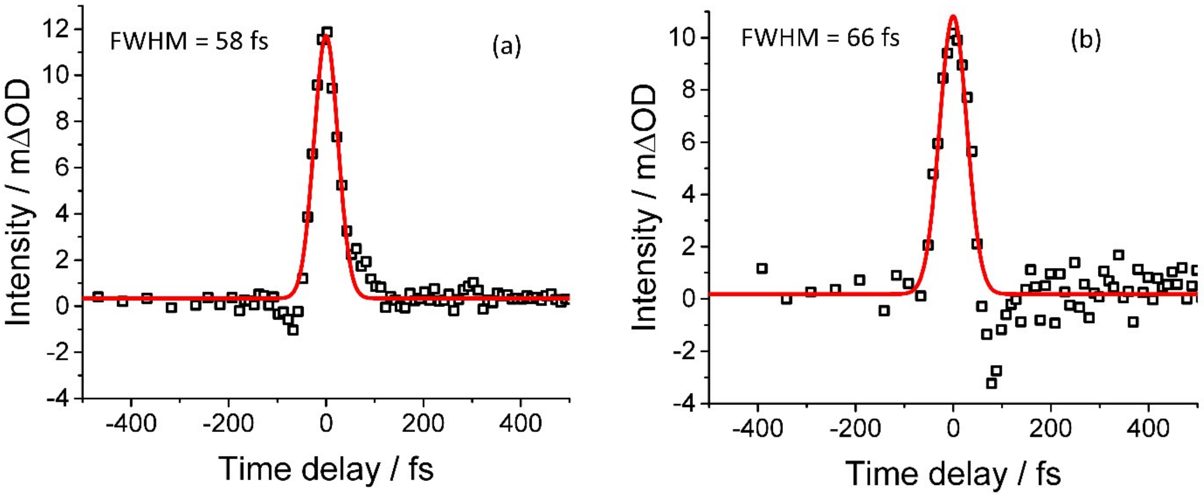

Figure 3: Response of (a) cyclohexane after pump irradiation at 290 nm and (b) methanol after pump irradiation at 308 nm. The signal corresponds to the absorption response at the maximum intensity at t_0: 350 nm and 330 nm probe for cyclohexane and methanol respectively. The two data sets (black squares) are both fit with a Gaussian function (red traces).

Figure 3 presents the transient response obtained from only the solvent (methanol at 308 nm pump; cyclohexane at 290 nm pump) and CaF_2 windows of the Harrick cell. Globally, the signal does not present noticeable dynamics and, therefore, does not perturb the time-constants extracted from the global fitting (see main text for details). Moreover, because of the wings observed in both sides of the peak, in the two solvents, the temporal resolution is underestimated using the FWHM. However, the FWHM used in the global fits (see section VII), is allowed to float, and always returns a value under 100 fs, which agrees with the present data. We conclude that our temporal resolution is thus less than 100 fs across the spectral window of our white light probe.

V. Fits of gas-phase transients to two exponential decays

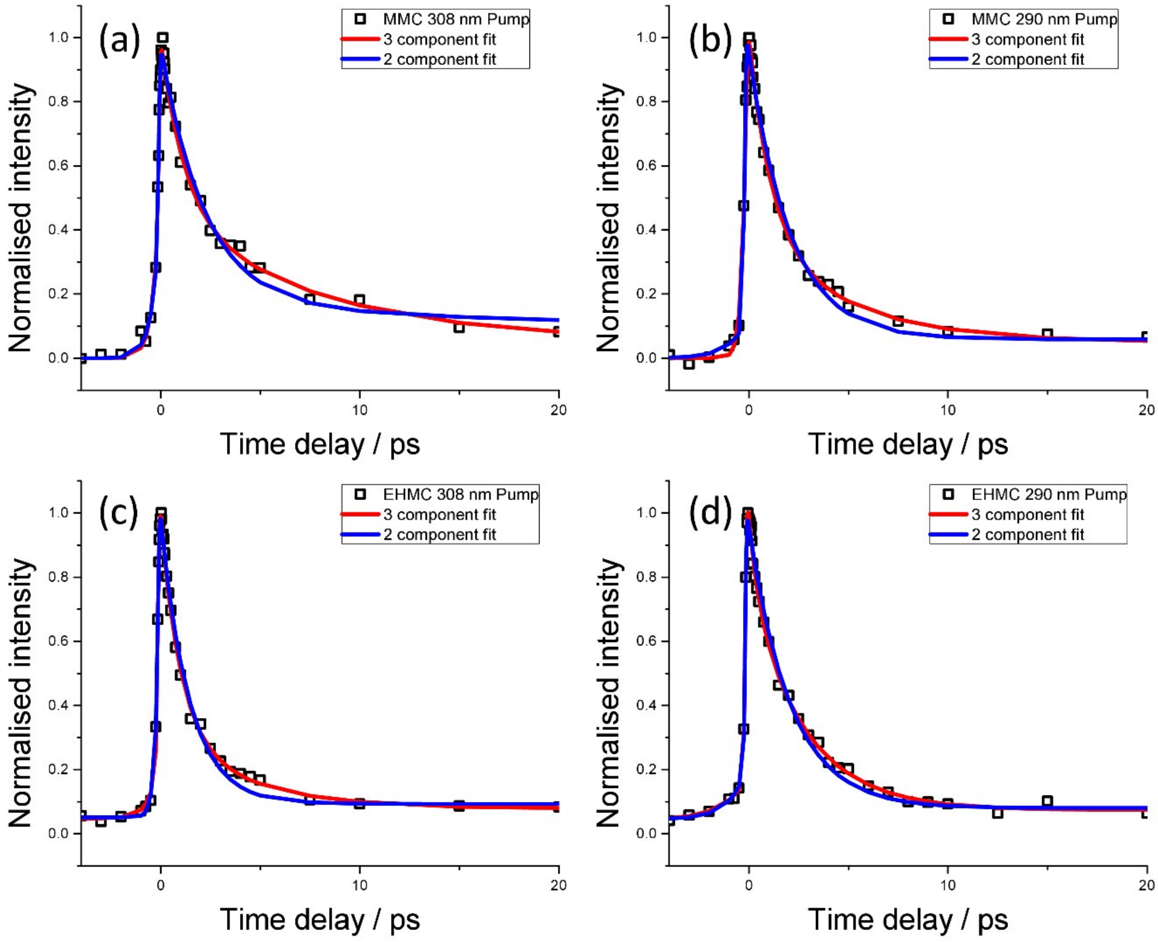

Figure 4: Gas-phase transients of (a) MMC after pump irradiation at 308 nm, (b) MMC after pump irradiation at 290 nm, (c) EHMC after pump irradiation at 308 nm and (d) EHMC after pump irradiation at 290 nm. The data sets (black squares) are all fit with a bi-exponential (blue traces) and tri-exponential (red traces) decay function.

Figure 4 presents transients taken for MMC and EHMC fit to two and three exponential decay functions. It can clearly be seen that, in all cases, three exponential decays present a better fit than two.

VI. TR-IY of *E*-MMC using the 315 nm probe

The two time-constants associated to the change of state from the $1^1\pi\pi^*$ to the $1^1n\pi^*$ obtained by fitting the TR-IY transient of *E*-MMC$^+$ in the gas-phase with 200 nm probe are in contrast to the values observed by Miyazaki *et al*. (see reference 26 in the main text). Indeed, our results do not show the ps-long time-constants and their energy-dependence these authors observed: timescales decrease from 280 to 13 ps (depending on which rotamer and vibronic state therein, was photoexcited) with increasing excitation energy, which ranges from 32328 to 33155 cm^{-1}.

To reconcile these differences, we performed TR-IY experiments with λ_{pump} = 308 nm and probing with the same wavelength as Miyazaki *et al*.: at 315 nm, just above the ionisation threshold. The data is presented in Figure 5. We fit the data with three exponential decays: τ_A = 0.6 ± 0.1 ps, τ_B = 13 ± 2 ps and τ_C = 400 ± 200 ps. τ_A and τ_B are in reasonable accord with τ_1 and τ_2 (1.1 ± 0.3 ps and 8 ± 2 ps, see main text), but a new time-constant, τ_C, is clearly needed for the fit to follow the trend of the data at Δt >50 ps. The small amplitude (comparatively to the short-time dynamics signal) at time delays greater than 50 ps and the fact that we are exciting multiple vibrational states (due to the spectral bandwidth of our laser) with different associated time-constants leads to a large error in τ_C. However, from the above argument, we are confident that our results show, by and large, the same long-time behaviour (within error) as Miyazaki *et al*.

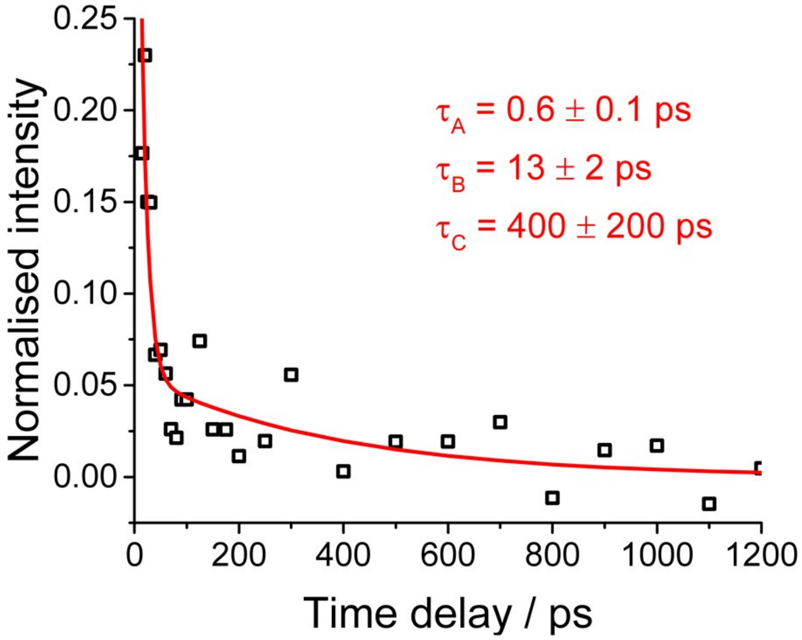

Figure 5: TR-IY transient (black squares) of *E*-MMC$^+$ upon 308 nm excitation using a 315 nm probe, along with a three time-constant fit (red trace).

VII. Detailed difference spectrum of *E*-MMC in methanol

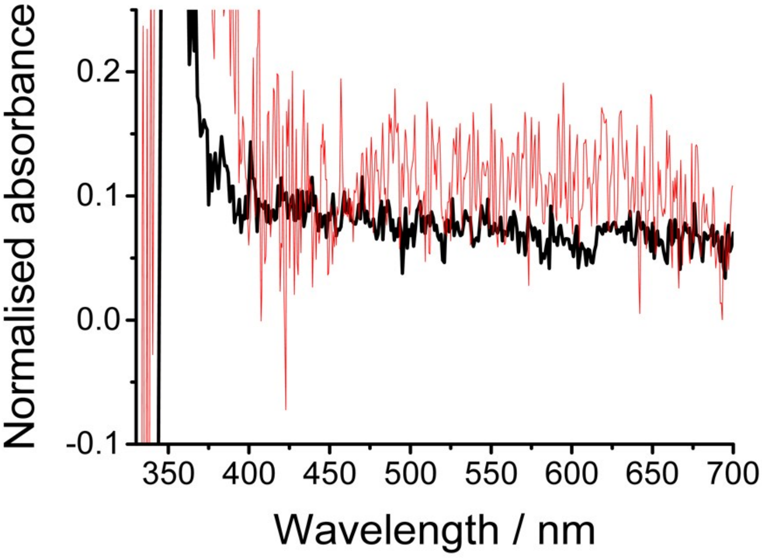

Figure 6: Smoothed (5 points) TAS (red trace) at 2 ns compared with the corresponding normalised difference spectrum (black trace) for *E*-MMC in methanol at maximum absorption pump irradiation (308 nm). The data is zoomed in intensity (from -0.1 to 0.25) to show the feature at ~600 nm.

VIII. Global fitting: residuals and uncertainties

Raw data and residuals of global fits:

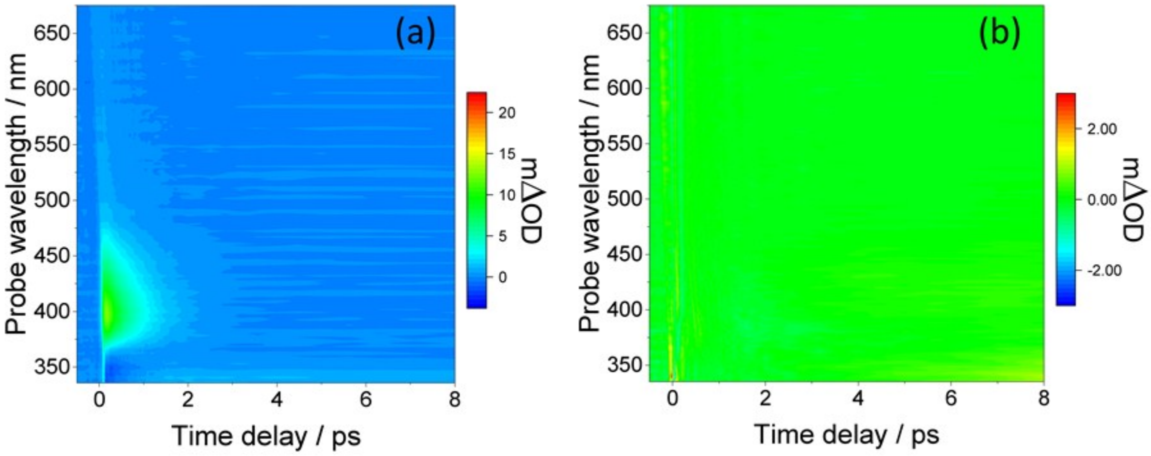

Figure 7: (a) TAS spectra of *E*-MMC in cyclohexane with a 308 nm pump irradiation and (b) associated residual fit.

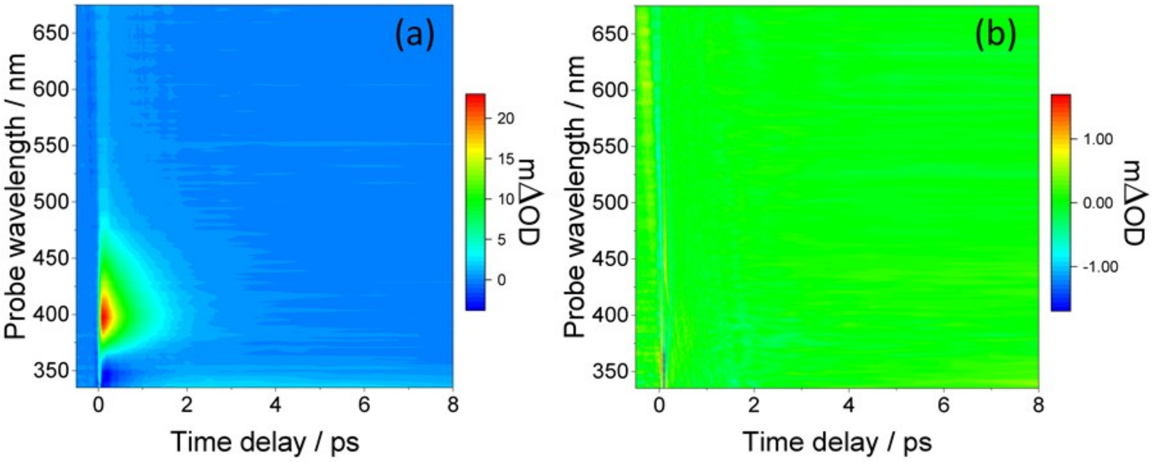

Figure 8: (a) TAS spectra of *E*-MMC in cyclohexane with a 290 nm pump irradiation and (b) associated residual fit.

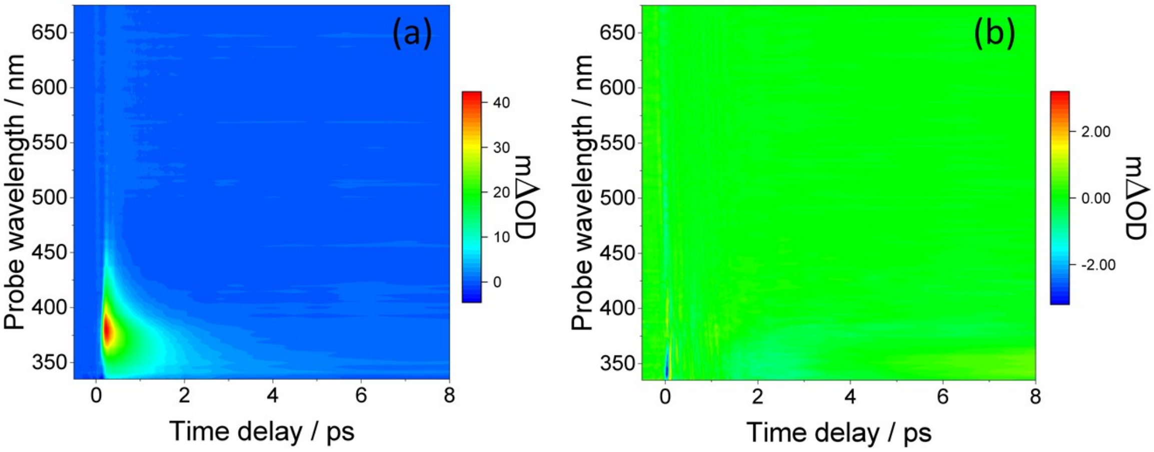

Figure 9: (a) TAS spectra of *E*-MMC in methanol with a 308 nm pump irradiation and (b) associated residual fit.

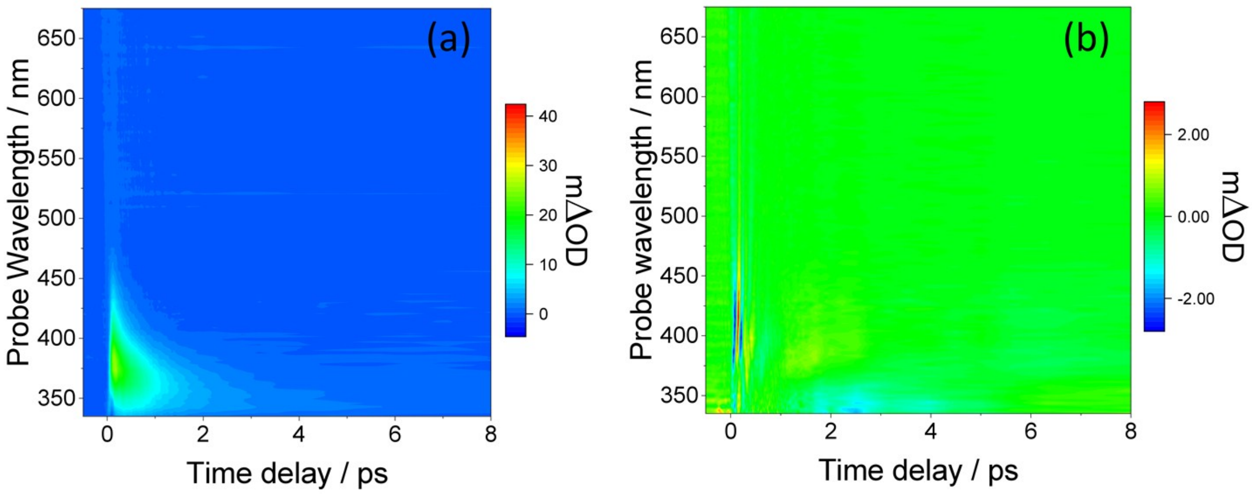

Figure 10: (a) TAS spectra of *E*-MMC in methanol with a 290 nm pump irradiation and (b) associated residual fit.

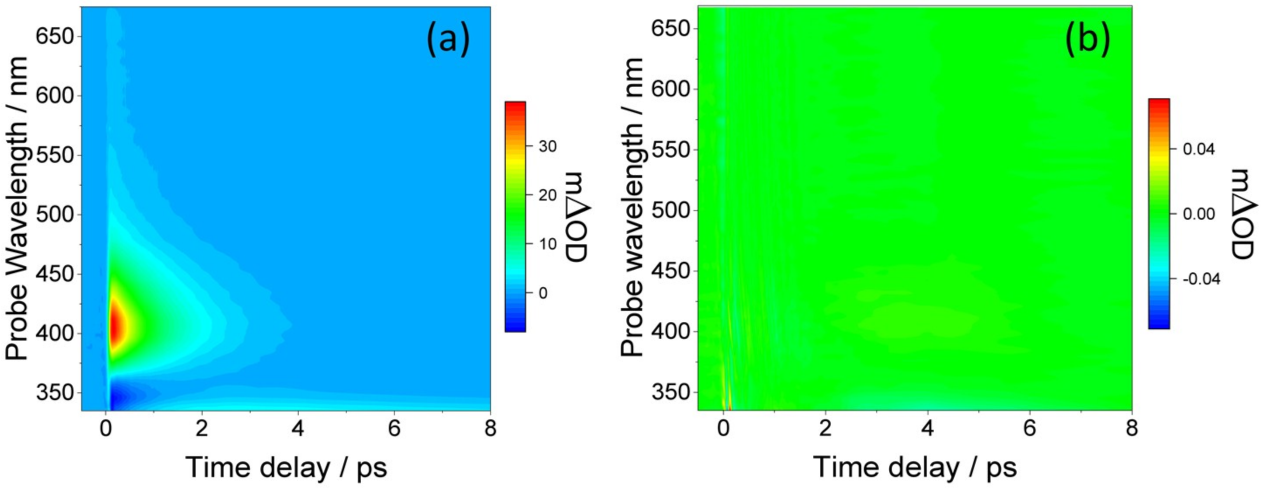

Figure 11: (a) TAS spectra of *E*-EHMC in cyclohexane with a 308 nm pump irradiation and (b) associated residual fit.

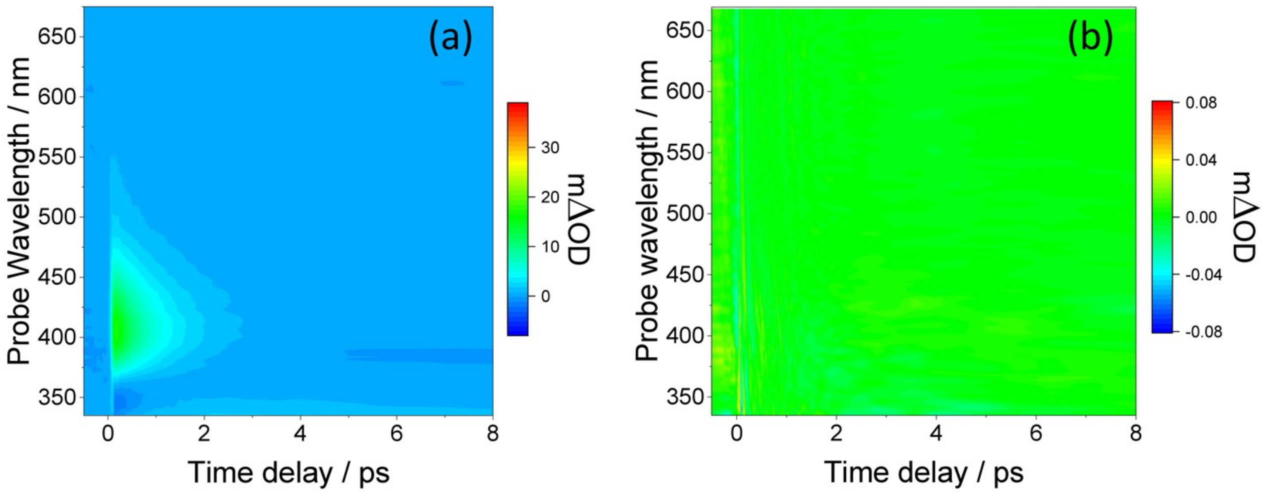

Figure 12: (a) TAS spectra of *E*-EHMC in cyclohexane with a 290 nm pump irradiation and (b) associated residual fit.

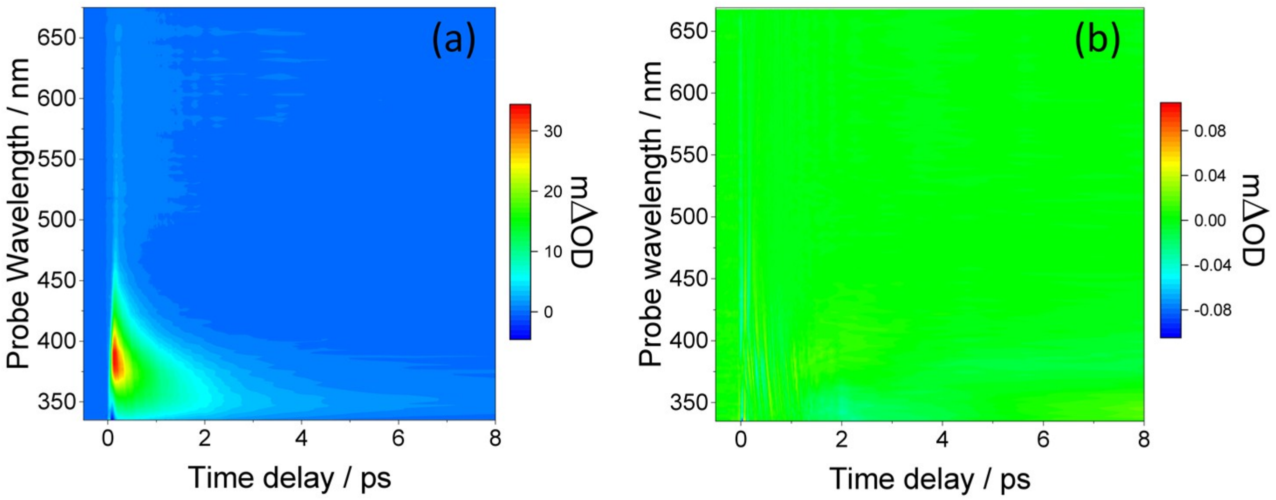

Figure 13: (a) TAS spectra of *E*-EHMC in methanol with a 308 nm pump irradiation and (b) associated residual fit.

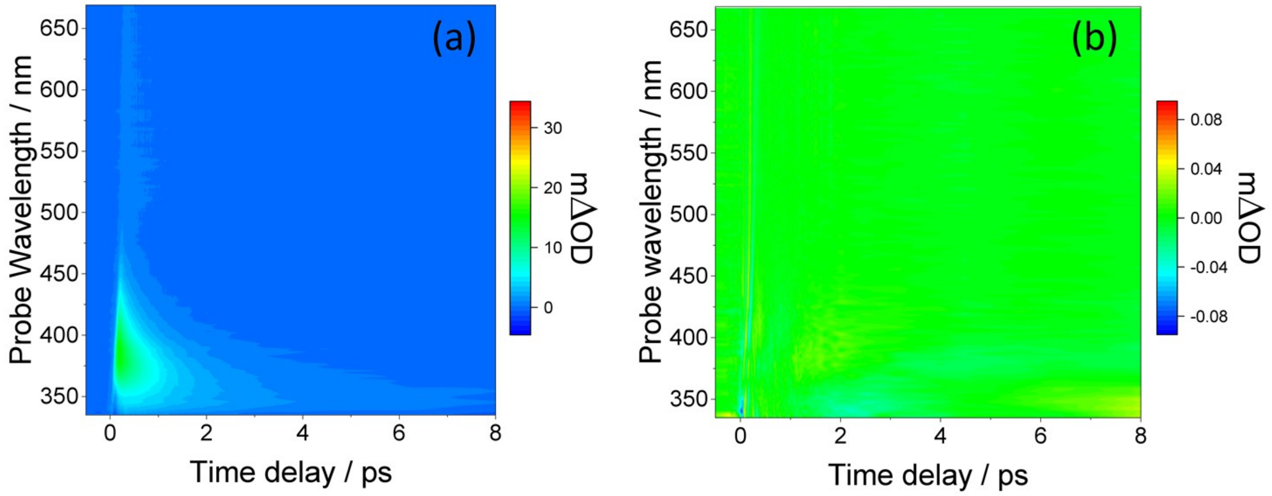

Figure 14: (a) TAS spectra of *E*-EHMC in methanol with a 290 nm pump irradiation and (b) associated residual fit.

Extracted time-constants and associated errors:

Table 1: Time-constants extracted from the global fitting of solution-phase TAS, after 308 nm and 290 nm excitation, in cyclohexane and methanol, both for *E*-MMC and for *E*-EHMC.

Compound / Solvent	Wavelength	τ_1 / ps	τ_2 / ps	τ_3 / ns
E-MMC / Cyclohexane	λ_{pump} = 308 nm	0.63 ± 0.02		>2.0
	λ_{pump} = 290 nm	0.62 ± 0.02		>2.0
E-MMC / Methanol	λ_{pump} = 308 nm	0.22 ± 0.04	0.75 ± 0.09	>2.0
	λ_{pump} = 290 nm	0.20 ± 0.02	0.89 ± 0.09	>2.0
E-EHMC / Cyclohexane	λ_{pump} = 308 nm	0.68 ± 0.08	2.1 ± 0.8	>2.0
	λ_{pump} = 290 nm	0.6 ± 0.1	1.8 ± 1.2	>2.0
E-EHMC / Methanol	λ_{pump} = 308 nm	0.26 ± 0.09	1.1 ± 0.3	>2.0
	λ_{pump} = 290 nm	0.25 ± 0.04	1.0 ± 0.2	>2.0

Uncertainties:[2-4]

Support plane analysis is used to calculate the uncertainties to the 95% level on the global fitted values reported in the article. For each dynamical process to which an error is assigned, its value is systematically varied. The goodness of fit, χ^2, is calculated and the remaining free parameters are optimised to minimise the residuals. In the case of *E*-MMC in methanol measurements and *E*-EHMC both in methanol and cyclohexane, where two time constants correspond to dynamical processes and errors are assigned, both lifetimes are varied systematically together. The goodness of fit is then normalised by that of the global minimum, χ^2_{min}, which allows a 95% confidence interval to be defined as:

$$\frac{\chi^2}{\chi^2_{min}} = 1 + \frac{p}{v}F(0.95,p,v)$$

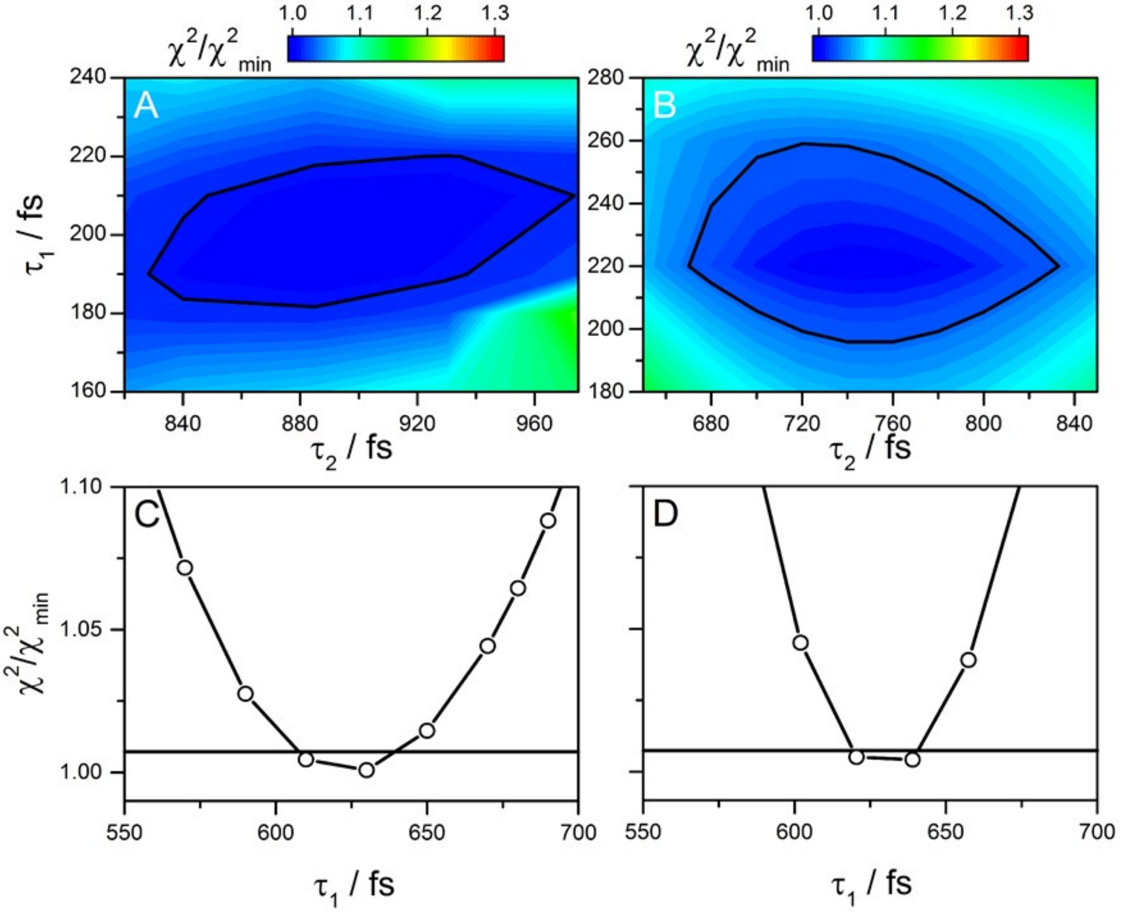

Figure 15: Support plane analysis for (A) *E*-MMC-methanol 290 nm, (B) *E*-MMC-methanol 308 nm. The black line indicates the boundary of the 95% confidence interval. (C) Similar analysis for *E*-MMC-cyclohexane at 290 nm and (D) *E*-MMC-cyclohexane at 308 nm. For *E*-MMC-cyclohexane, only one lifetime was varied given all of the dynamical processes were far removed from each other. The horizontal line represents the 95% confidence interval.

---

[2] S. C. Warren, A. Margineanu, D. Alibhai, D. J. Kelly, C. Talbot, Y. Alexandrov, I. Munro, M. Katan, C. Dunsby and P. M. W. French, *PLoS ONE*, 2013, **8**, e70687.

[3] T. A. Roelofs, C. H. Lee and A. R. Holzwarth, *Biophys. J.*, 1992, **61**, 1147.

[4] J. R. Lakowicz, *Principles of Fluorescence Spectroscopy Third Edition*, Springer, Singapore, 2011.

where p is the number of parameters in the global fit, υ is the number of degrees of freedom and F is the inverse F cumulative distribution function. The final reported uncertainties are that which deviate by the greatest value relative to the global minimum lifetimes, with this then taken to be symmetric about the global minimum. Qualitatively, the uncertainties are shown in Figures 14 and 15, for *E*-MMC and *E*-EHMC respectively, and quantitatively given in Table 1.

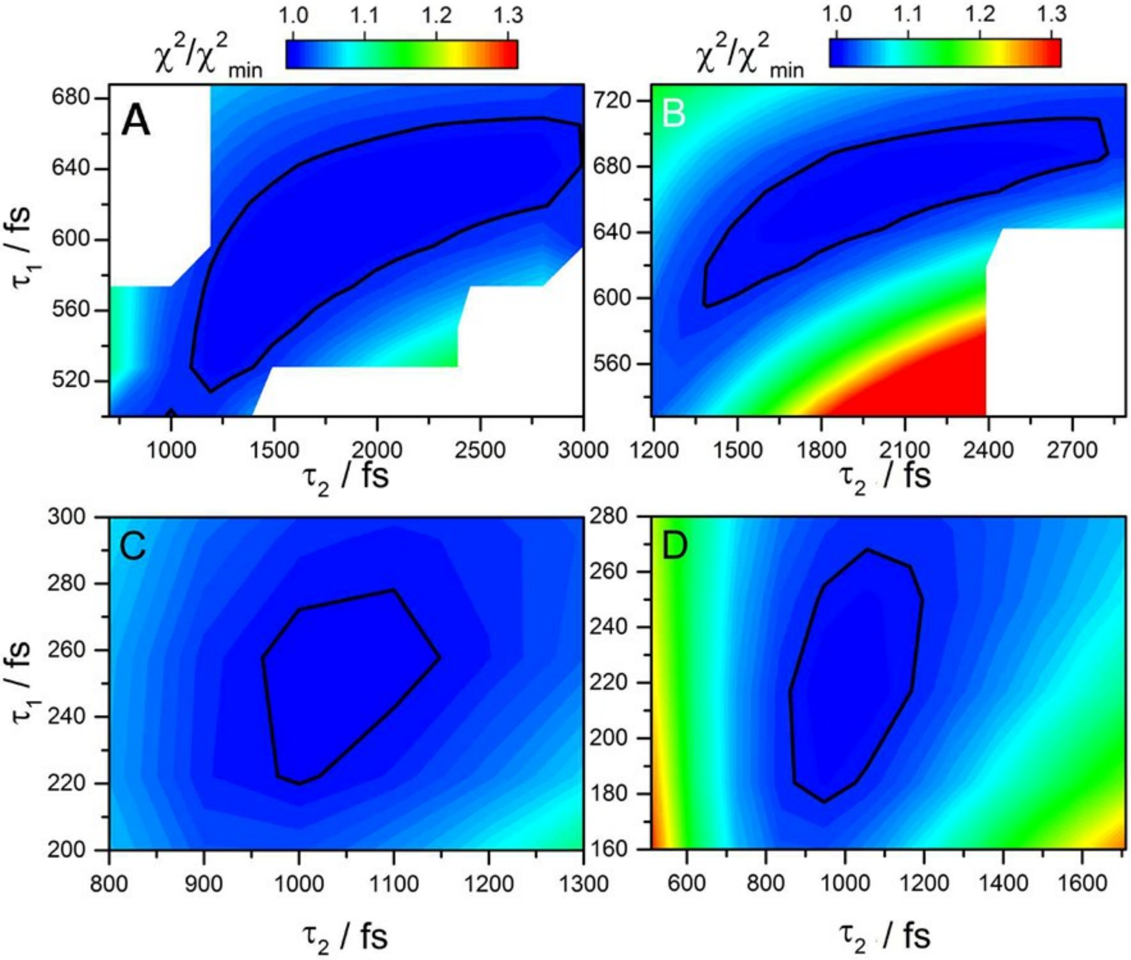

Figure 16: Support plane analysis for (A) *E*-EHMC-cyclohexane 290 nm, (B) *E*-EHMC-cyclohexane 308 nm. The black line indicates the boundary of the 95% confidence interval. (C) Similar analysis for *E*-EHMC-methanol at 290 nm and (D) *E*-EHMC-cyclohexane at 308 nm. Part of the surfaces on A and B are white because we didn’t explore these regions as the 95% confidence interval was already found.

IX. NMR spectra of sample pre- and post-irradiation

Figure 16 shows the assigned ^1H NMR ($CDCl_3$, 400 MHz) of MMC samples prior to irradiation. The starting material was the *E* isomer exclusively, evidenced by the 16 Hz $^3J_{H\text{-}H}$ coupling of the doublet of protons 2e and 3e as well as the lack of any *Z* protons. Upon irradiation, the *Z* isomer was clearly present in the sample, as shown in Figures 17 and 18.

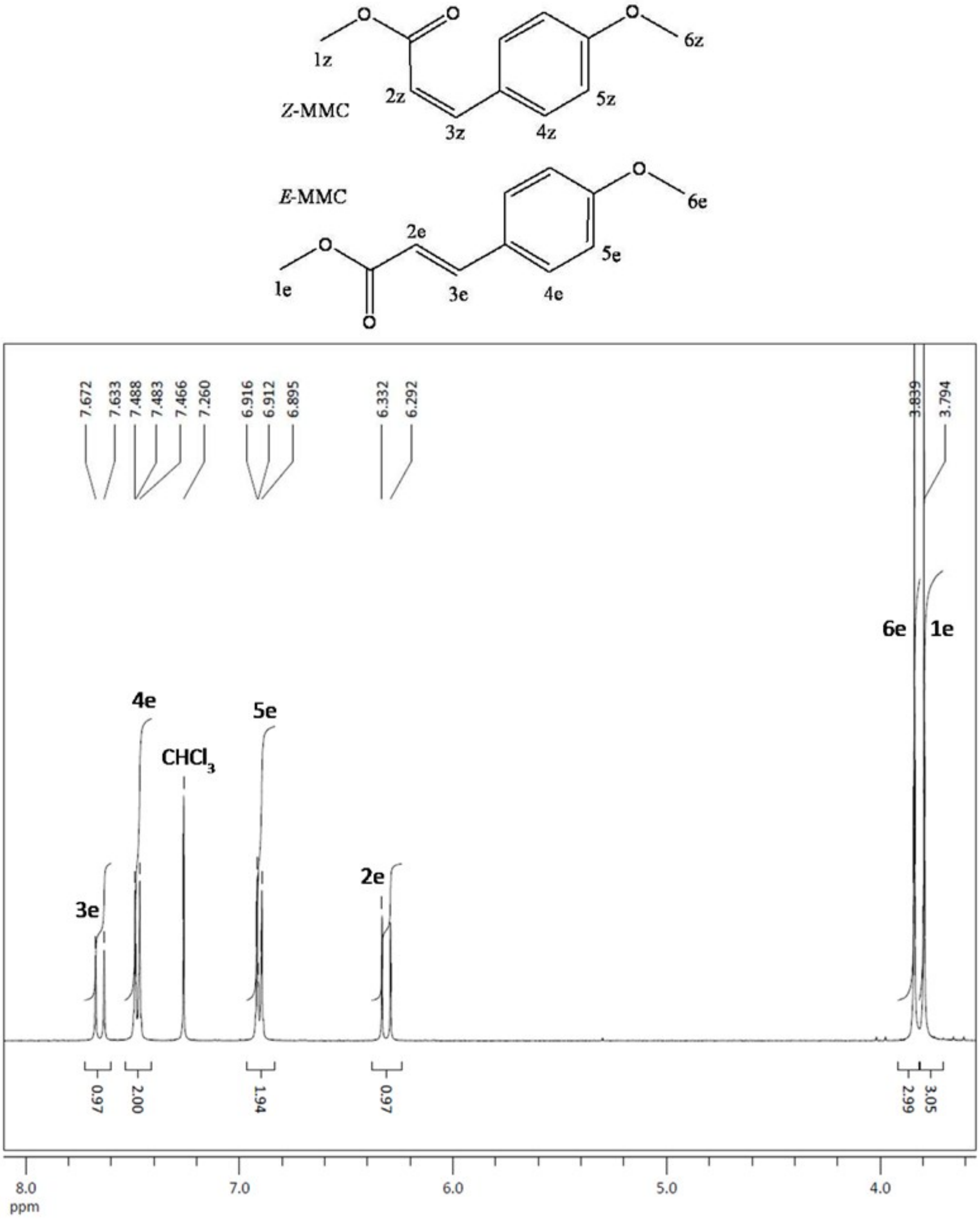

Figure 17: ^1H NMR of *E*-MMC (~5.2 mM) prior to irradiation, in $CDCl_3$ at 400 MHz, and peak attribution; for the peaks at ~6.3 and ~7.6 ppm a value of $^3J_{3\text{-}2}$(e)=16 Hz is determined.

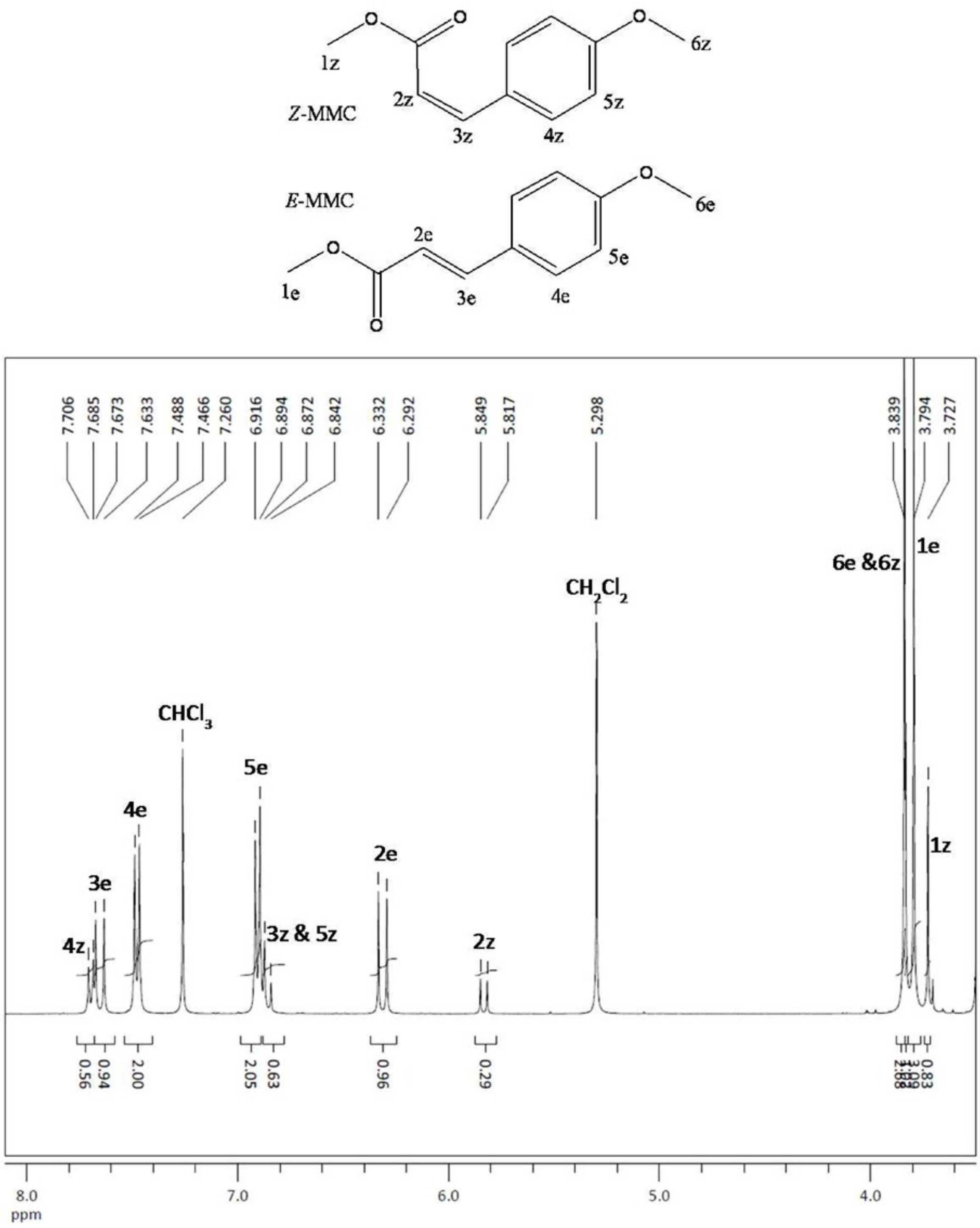

Figure 18: ^{1}H NMR of *E*-MMC (~5.2 mM), after one hour of irradiation at 290 nm in cyclohexane, performed in chloroform at 400 MHz, and peak attribution; a value of $^3J_{3\text{-}2}(z)$=13 Hz is determined for the peak at ~5.8 ppm and for the peaks at ~6.3 and ~7.6 ppm a value of $^3J_{3\text{-}2}(e)$=16 Hz is determined.

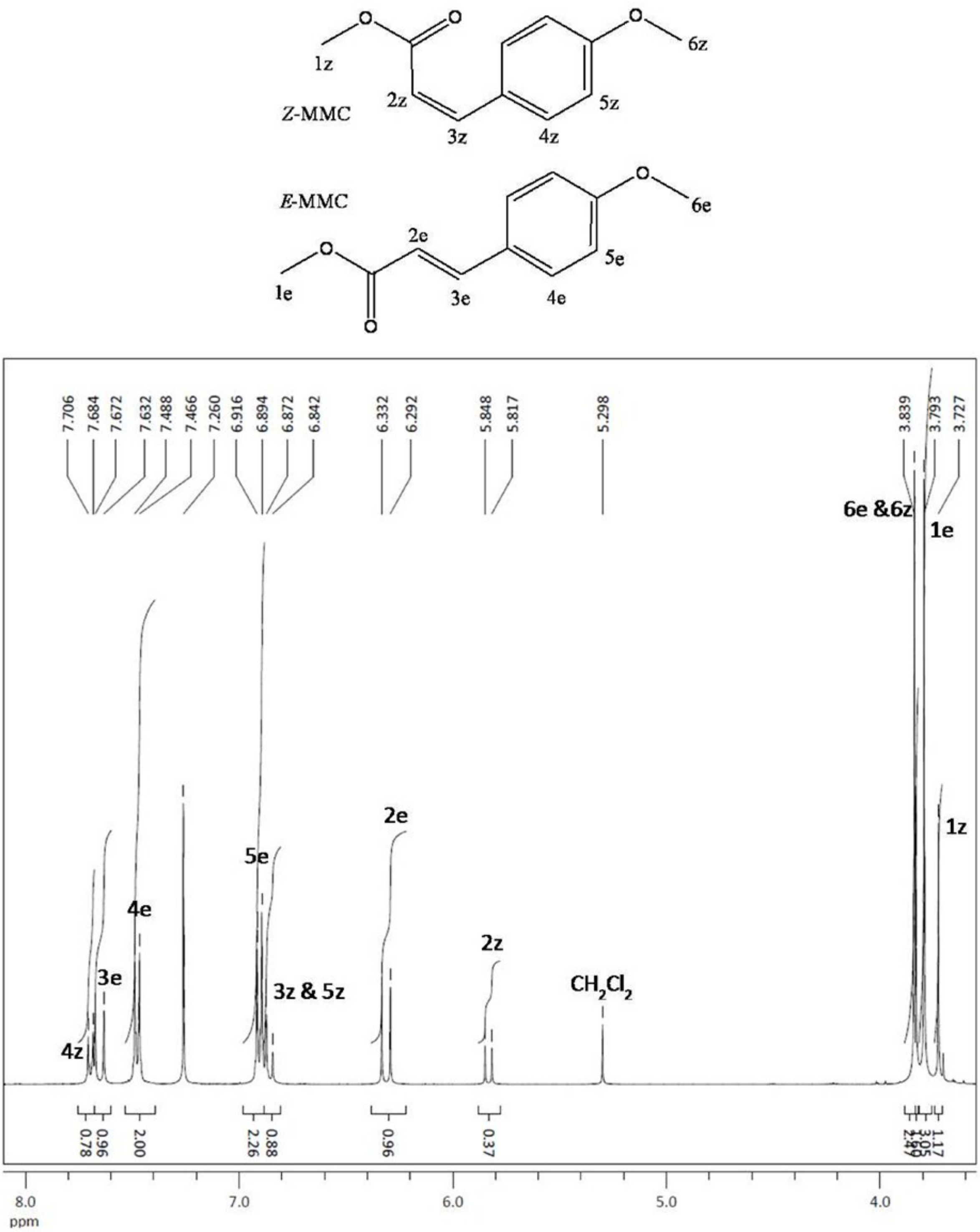

Figure 19: ^{1}H NMR of *E*-MMC (~5.2 mM), after one hour of irradiation at 308 nm in methanol, performed in chloroform at 400 MHz, and peak attribution; a value of $^3J_{3\text{-}2}$(z)=13 Hz is determined for the peak at ~5.8 ppm and a value of $^3J_{3\text{-}2}$(e)=16 Hz is determined for the peaks at ~6.3 and ~7.6 ppm.

The reasoning for the presence of *Z* isomers are: i) the $^3J_{H\text{-}H}$coupling changed from 16 Hz (2e & 3e) to 13 Hz (2z & 3z), typical of *Z* alkene protons; ii) both of the alkene protons were shifted upfield; and iii) the lack of new identifiable species as well as the consistent ratio between respective integrated peaks.

We can then estimate the *E*/*Z* isomer ratio by determining the ratio of the integral of the respective species. However, as shown in the spectra, there is significant overlap for most of the peaks except for protons 4e, 2e and 2z, therefore the total integral for each species was achieved by fixing the integral of proton 4e to a value of 2, as shown in Figures 17 and 18. Integrated number and final content of isomer *Z* are listed in Table 2.

Table 2: Integrated number and final content of isomer Z for MMC isomers, both in methanol and cyclohexane, relative to proton 4.

Proton	Cyclohexane		Methanol	
	E	*Z*	*E*	*Z*
1	3.09	0.83	3.05	1.17
2	0.96	0.29	0.96	0.37
3	0.94	2.68*	0.96	3.14*
4	2	0.56	2	0.78
5	2.68*		3.14*	
6	3.70^{+}		4.07^{+}	
Z content	**21-23 %**		**27-29 %**	

* Both in methanol and cyclohexane the integrals corresponding to the protons 3z, 5e and 5z are overlapped. We therefore assign a unique value in both solvents and do not use them to calculate the *Z* content.

$^{+}$ Same as above: the peaks corresponding to protons 6e and 6z are overlapped.

The same study has been done with *E*-EHMC as presented in Figures 19, 20 and 21.

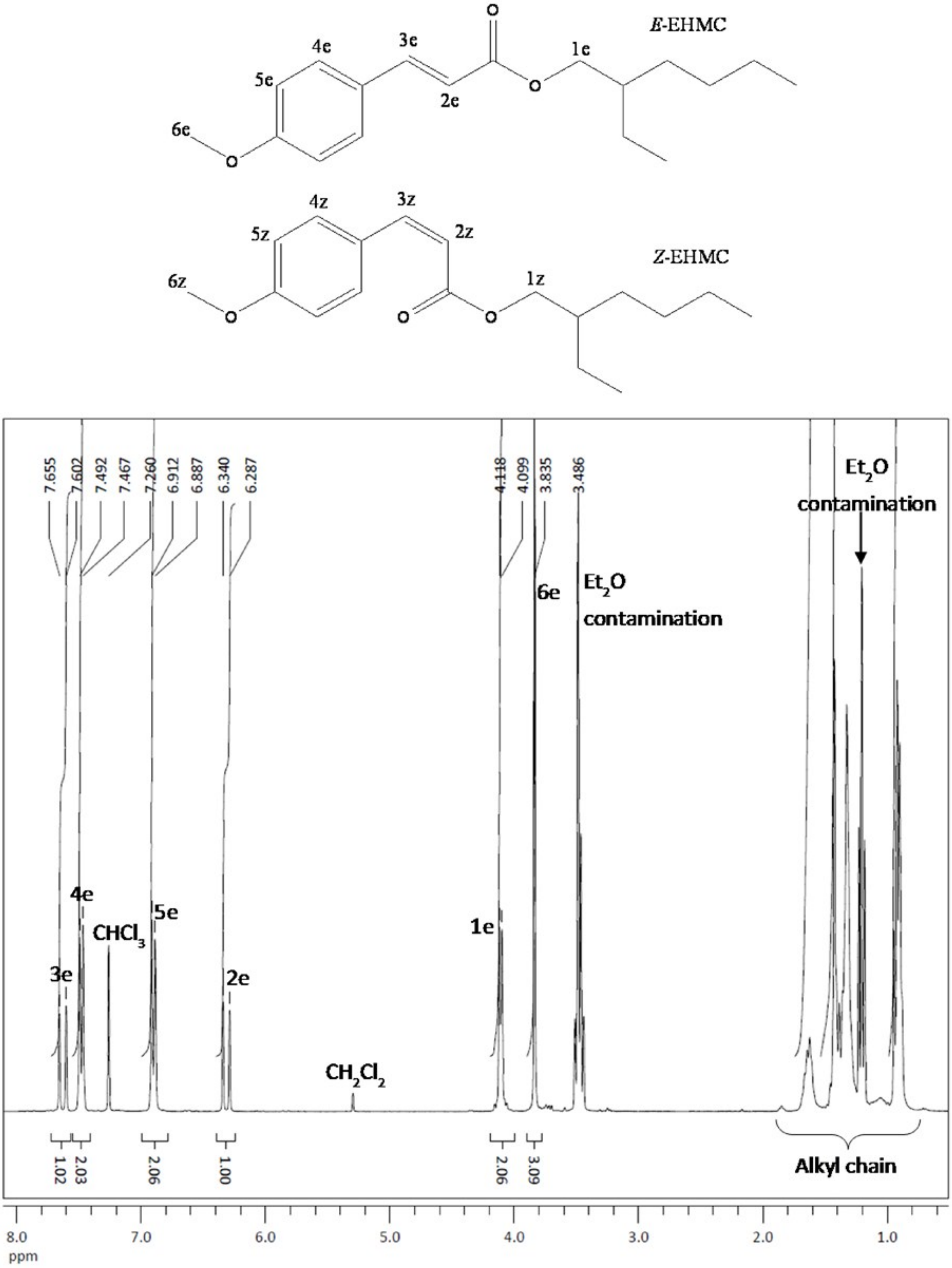

Figure 20: ^{1}H NMR of *E*-EHMC (~5.2 mM) prior to irradiation, in chloroform at 300 MHz, and peak attribution; for the peaks at ~6.3 and ~7.6 ppm a value of $^3J_{3\text{-}2}$(e)=16 Hz is determined.

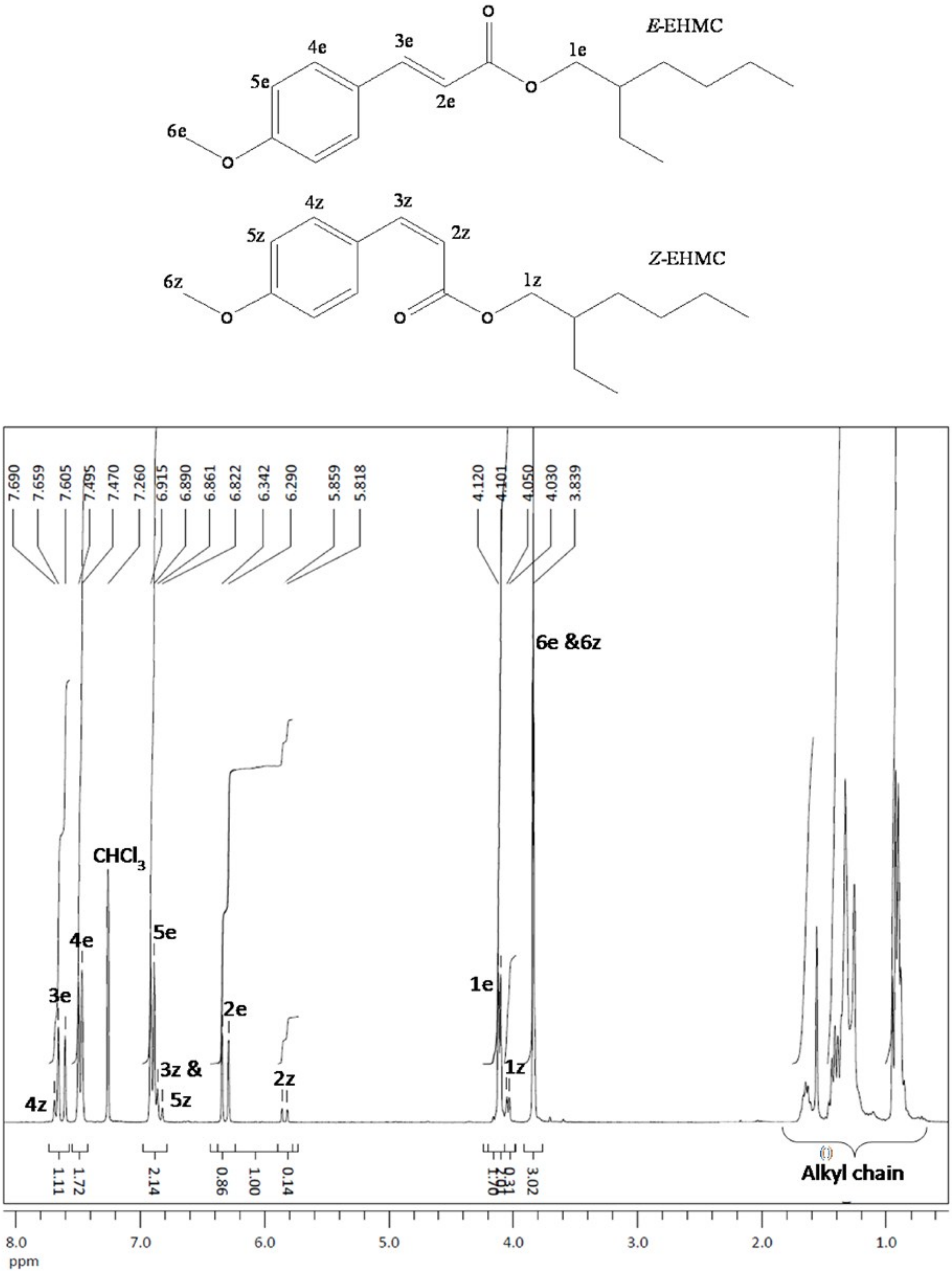

Figure 21: ^{1}H NMR of *E*-EHMC (~5.2 mM), after one hour of irradiation at 290 nm in cyclohexane, performed in chloroform at 300 MHz, and peak attribution; for the peak at ~5.8 ppm a value of $^3J_{3\text{-}2}(z)=13$ Hz is determined and for the peak at ~6.3 ppm a value of $^3J_{3\text{-}2}(e)=16$ Hz is determined.

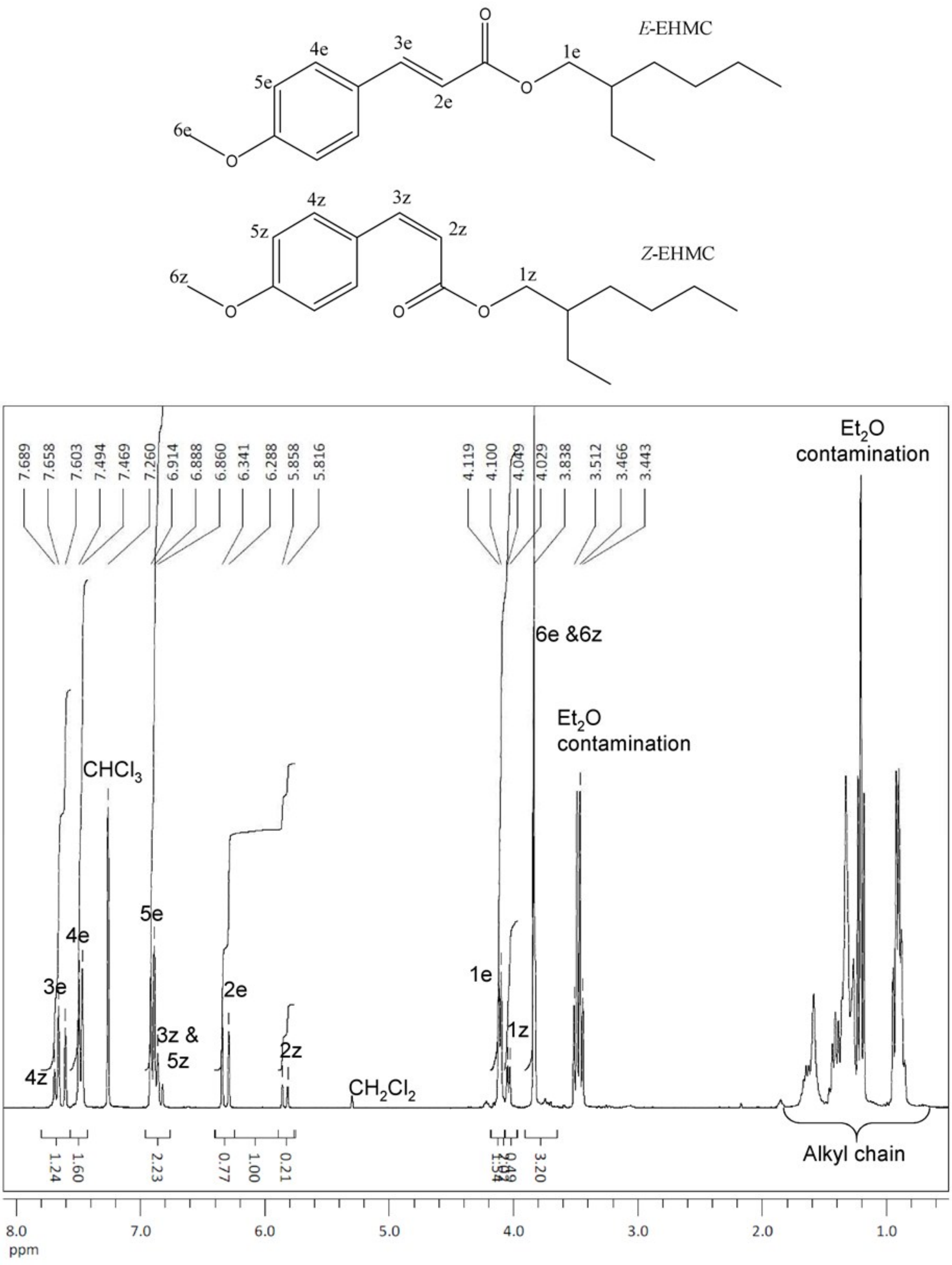

Figure 22: ^{1}H NMR of *E*-EHMC (~5.2 mM), after one hour of irradiation at 308 nm in methanol, performed in chloroform at 300 MHz, and peak attribution; for the peak at ~5.8 ppm a value of $^3J_{3\text{-}2}(z)=13$ Hz is determined and for the peak at ~6.3 ppm a value of $^3J_{3\text{-}2}(e)=16$ Hz is determined.

Table 3: Integrated number and final content of isomer Z for EHMC isomers, both in methanol and cyclohexane, relative to proton 4.

Proton	Cyclohexane		Methanol	
	E	*Z*	*E*	*Z*
1	1.70	0.31	1.54	0.49
2	0.86	0.14	0.77	0.21
3	1.11$^\$$	2.14*	1.24$^\$$	2.23*
4	1.72	1.11$^\$$	1.60	1.24$^\$$
5	2.14*		2.23*	
6	3.02$^+$		3.20$^+$	
Z content	**14-15 %**		**21-24 %**	

* Both in methanol and cyclohexane the integrals corresponding to the protons 3z, 5e and 5z are overlapped. We therefore assign a unique value in both solvents and do not use them to calculate the *Z* content.

$^+$ Same as above: the peaks corresponding to protons 6e and 6z are overlapped.

$^\$$ Same as above: the peaks corresponding to 3e and 4z are overlapped.

X. Line-outs of *E*-MMC and *E*-EHMC TAS in methanol at 450 nm

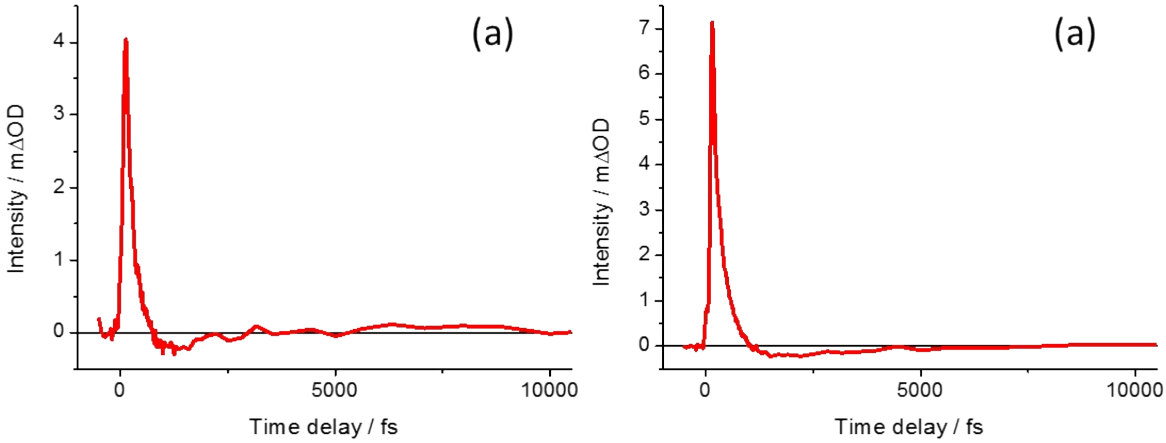

Figure 23: Transients from (a) *E*-MMC and (b) *E*-EHMC in methanol at 450 nm, hν_{pu} = 308 nm. A negative intensity can be seen around 2 ps due to stimulated emission from the excited state.